CrossMark

Formation of Lunar Basins from Impacts of Leftover Planetesimals

David Nesvorný[1] , Fernando V. Roig[2] , David Vokrouhlický[3] , William F. Bottke[1] , Simone Marchi[1] ,
Alessandro Morbidelli[4], and Rogerio Deienno[1]

[1] Department of Space Studies, Southwest Research Institute, 1050 Walnut Street, Suite 300, Boulder, CO 80302, USA; davidn@boulder.swri.edu
[2] Observatório Nacional, Rua Gal. Jose Cristino 77, Rio de Janeiro, RJ 20921-400, Brazil
[3] Institute of Astronomy, Charles University, V Holešovičkách 2, CZ18000 Prague 8, Czech Republic
[4] Laboratoire Lagrange, UMR7293, Université Côte d'Azur, CNRS, Observatoire de la Côte d'Azur, Bouldervard de l'Observatoire, F-06304, Nice Cedex 4, France

Abstract

The Moon holds important clues to the early evolution of the solar system. Some 50 impact basins (crater diameter $D > 300$ km) have been recognized on the lunar surface, implying that the early impact flux was much higher than it is now. The basin-forming impactors were suspected to be asteroids released from an inner extension of the main belt (1.8–2.0 au). Here we show that most impactors were instead rocky planetesimals left behind at $\sim$0.5–1.5 au after the terrestrial planet accretion. The number of basins expected from impacts of leftover planetesimals largely exceeds the number of known lunar basins, suggesting that the first $\sim$200 Myr of impacts are not recorded on the lunar surface. The Imbrium basin formation (age $\simeq$3.92 Gyr; impactor diameter $d \gtrsim 100$ km) occurs with a 15%–35% probability in our model. Imbrium must have formed unusually late to have only two smaller basins (Orientale and Schrödinger) forming afterwards. The model predicts $\simeq$20 $d > 10$ km impacts on the Earth 2.5–3.5 Gyr ago (Ga), which is comparable to the number of known spherule beds in the late Archean.

Unified Astronomy Thesaurus concepts: Solar system formation (1530); Lunar impacts (958)

1. Introduction

In the standard model of terrestrial planet formation (Wetherill 1990), accretional collisions between 1 and 1000 km planetesimals lead to gradual build up of lunar-to-Mars-size protoplanets that gravitationally interact and further grow during the late stage of giant impacts (Chambers & Wetherill 1998). Hafnium–tungsten (Hf–W) isotopic system analyses indicate that the Moon-forming impact on proto-Earth happened $t = 30$–150 Myr after the appearance of the first solar system solids $T \simeq 4.57$ Ga (Kleine & Walker 2017). The newborn Moon was molten, gradually cooled down, and was eventually able to support impact structures on its surface. This is time zero for the lunar crater record. The lunar surface recorded $\simeq$50 basin-scale impacts of $d > 20$ km bodies (Miljković et al. 2016) since time zero, at least some of which formed relatively late. The radiometric dating of Apollo impact melts indicates that the Imbrium basin, which dominates the lunar near side, formed at $t \simeq 650$ Myr (Zhang et al. 2019). From all other lunar basins only Orientale and Schrödinger have lower accumulated density of superposed craters than Imbrium (Fassett et al. 2012), and must therefore be younger.

Having (at least) three basin-forming impacts happening at $t \gtrsim 650$ Myr is unexpected from the planet formation perspective because in the inner solar system, where the accretion processes have relatively short timescales (<100 Myr), the impact flux should have rapidly declined over time. The ubiquity of $\sim$3.9 Gyr ages in the Apollo samples has therefore motivated the impact spike hypothesis where it was assumed that the Imbrium-era impacts mark an epoch of enhanced bombardment (Tera et al. 1974), and prompted a search for possible causes. For example, it has been suggested that a dynamical instability in the outer solar system—if it happened suitably late—could have destabilized asteroid and comet reservoirs, and produced an Imbrium-era spike (Gomes et al. 2005). The late-instability model, however, has fundamental problems with the survival of the terrestrial planets (Kaib & Chambers 2016; e.g., the fully formed Earth often collides with Venus) and the delay itself (Nesvorný et al. 2018), leaving the problem of the origin of lunar basins unresolved.

To settle this matter, we construct a physical model for three key populations of impactors in the inner solar system: (i) leftover planetesimals in the terrestrial planet zone (0.3–1.75 au), (ii) main-belt asteroids (1.75–4 au), and (iii) comets. The model is based on N-body simulations of planets and small bodies over the age of the solar system (Section 2). The simulations follow the growth of terrestrial planets, collisional and dynamical decline of populations, and record impacts of (i)–(iii) on the terrestrial worlds. For consistency, they include the outer planet instability (Tsiganis et al. 2005)—a brief period in the early solar system when the giant planets were scattered to their current orbits. The instability is assumed to happen within $t \sim 10$ Myr after the protoplanetary gas disk dispersal (Clement et al. 2018). We note that the nature and timing of the instability are inconsequential for the main results presented here.

2. Methods

2.1. Leftover Planetesimals

We adopt the terrestrial planet accretion model from Nesvorný et al. (2021b), where protoplanets started in a narrow annulus ($r = 0.7$–1 au) and planetesimals in a wider belt ($r \simeq 0.5$–1.5 au). The model accounted for the planetesimal-driven migration and dynamical instability of the outer planets (Tsiganis et al. 2005). In the simulation highlighted here, the instability happened at $\simeq$5.8 Myr and the Moon-forming impact happened at $\simeq$40 Myr after the gas disk dispersal,

when two roughly equal-mass protoplanets—each with mass $\simeq 0.5$ $M_{\rm Earth}$—collided. The timing of the Moon-forming impact satisfies constraints from Hf–W isotope systematics (Kleine & Walker 2017). The low speed collision between two nearly equal-mass protoplanets falls into the preferred regime of Moon-forming impacts (Canup et al. 2022). The masses and orbits of the terrestrial planets were accurately reproduced in the simulations (Nesvorný et al. 2021b).

To determine the impact flux of leftover planetesimals on the terrestrial worlds we recorded the orbits of planets and planetesimals in the original simulations shortly after the Moon-forming impact. The planetesimals in the asteroid belt region were ignored (see below for asteroids). Mercury was not included to speed up the integrations; all other planets, Venus to Neptune were accounted for. We assumed that the terrestrial worlds were fully grown after the Moon-forming impact and their masses did not subsequently change. To increase the model statistics, each planetesimal was cloned by slightly altering the velocity vector ($<10^{-6}$ fractional change). In total, we had nearly 130,000 planetesimal clones. The N-body integrator swift_rmvs4 (Levison & Duncan 1994) was used to follow the system of planets and planetesimals over 1 Gyr. All impacts of planetesimals on planets were recorded by the integrator. The lunar impacts—the Moon was not included in the simulations—were obtained by rescaling the results from Earth's impacts (the gravitational focusing factors were computed from velocities recorded by swift_rmvs4).

We used the Boulder code (Morbidelli et al. 2009) to model the collisional evolution of planetesimals. Boulder employs a statistical particle-in-the-box algorithm that is capable of simulating collisional fragmentation of planetesimal populations. The main input parameters of the Boulder code are: (i) the initial size distribution of the simulated populations, (ii) intrinsic collision probability $p_{\rm i}$, and (iii) mean impact speed $v_{\rm i}$. For (i), we adopted a broken power law $N(>d) \propto d^{-\gamma}$ with $\gamma = 1.5$ for $d < d^*$ and $\gamma = 5$ for $d > d^*$, and $d^* \sim 100$ km (Youdin & Goodman 2005, Morbidelli et al. 2009). We explored a wide range of initial masses ($0.001 < M_0 < 3$ $M_{\rm Earth}$). The probabilities $p_{\rm i}(t)$ and velocities $v_{\rm i}(t)$ of mutual collisions between planetesimals, both as a function of time, were computed from the terrestrial planet simulation described above.

The Boulder code was run to 1 Gyr. We found that the size distribution of planetesimals rapidly changed and reached an equilibrium shape by only ~ 20 Myr. The subsequent collisional evolution was insignificant because the planetesimal population was reduced by a large factor. In this sense, the shape of the size distribution of leftover planetesimals at the time of the Moon-forming impact, and any time after that, is a fossilized imprint of the intense collisional grinding that happened in the first ~ 20 Myr (Bottke et al. 2007). The equilibrium size distribution shows a break at $d \simeq 100$ km, a shallow slope for $d = 20$–100 km, and a slightly steeper slope for $d < 20$ km. It is similar to that of the (scaled) asteroid belt, just as needed to explain the size distribution of ancient lunar craters (Strom et al. 2005). The main variability in these results is caused by the assumptions about (i) and the planetesimal strength $Q^*_{\rm D}$ (e.g., Benz & Asphaug 1999). For example, we identified cases where the size distribution for $d = 10$–100 km was slightly steeper than that of the asteroid belt. The steeper distribution would help to alleviate the problem with the excess of superbasins (Minton et al. 2015).

The overall effect of collisional grinding depends on the initial mass M_0: stronger/weaker collisional grinding is found if M_0 was higher/lower. We characterized this dependence in detail (D. Nesvorný et al. 2022, in preparation). The stronger grinding for larger initial masses leads to a situation where the population of leftover planetesimals for $t > 20$ Myr does *not* sensitively depend on M_0. For $M_0 > 0.1$ $M_{\rm Earth}$, we estimate $\sim (2.6$–$5.2) \times 10^5$ $d > 10$ km planetesimals at $t = 40$ Myr and use this as the standard calibration in Section 3. The effects of collisional grinding are greatly reduced for $M_0 < 0.1$ $M_{\rm Earth}$, but the planetesimal population ended up to be smaller in this case (because it was already small initially). For $M_0 < 0.03$ $M_{\rm Earth}$, for example, we found $<10^5$ $d > 10$ km planetesimals at 40 Myr. This would imply an implausibly low probability of Imbrium formation ($<5\%$; Section 3).

2.2. Asteroids

A dynamical model for asteroid impactors was published in Nesvorný et al. (2017a). The model used the same setup for the planetesimal-driven migration and instability of the outer planets as the terrestrial planet formation model described above. To start with, the terrestrial planets were placed on the low-eccentricity and low-inclination orbits. The surface density profile of asteroids was assumed to follow $\Sigma(r) \propto r^{-1}$. The radial profile was smoothly extended from $r > 2$ au, where the model can be calibrated on observations of main-belt asteroids (see below), to $r = 1.75$–2 au. This fixed the initial number of bodies in the now largely extinct E-belt (Bottke et al. 2012). The results had large statistics (50,000 model asteroids) and full temporal coverage (4.57 Gyr).

The flux of asteroid impactors was calibrated from today's asteroid belt. We showed that the model distribution at the simulated time $t = 4.57$ Gyr (i.e., at the present epoch) was a good match to the orbital distribution of asteroids. The number of model $d > 10$ km asteroids at $t = 4.57$ Gyr was set to be equal to the number of $d > 10$ km main-belt asteroids ($\simeq 8200$), as measured by the Wide-field Infrared Survey Explorer (Mainzer et al. 2019). When propagated backward in time—using the simulation results—this provided the number of asteroids and asteroid impactors over the whole solar system history.

We empirically approximated the asteroid impact flux. In terms of the cumulative number of Earth impactors with diameters $>d$ at times $>t$, the best fit yields

$$F(d, t) = F_1(d)\exp[-(t/\tau)^\alpha] + F_2(d)T, \qquad (1)$$

with $\tau = 65$ Myr, $\alpha = 0.6$, $T = 4570 - t$, and t in Myr. The first term in Equation (1) accounts for the decline of asteroid impactors during early epochs. The second term represents the constant impact flux in the last 3 Gyr. There are two size-dependent factors in Equation (1). $F_1(d)$ is assumed to follow the size distribution of main-belt asteroids; the fit to simulation results gives $F_1(10\,{\rm km}) = 225$. Also, from the main-belt size distribution, $F_1(1\,{\rm km}) = 3.0 \times 10^4$. $F_2(d)$ is calibrated on modern near-Earth asteroids (NEAs). Nesvorný et al. (2021a) estimated ~ 3 impacts of $d > 10$ km NEAs on the Earth per Gyr; we thus have $F_2(10\,{\rm km}) = 3 \times 10^{-3}$ Myr^{-1}.

2.3. Comets

A dynamical model for comets was developed in Nesvorný et al. (2017b). To start with, a million cometesimals were
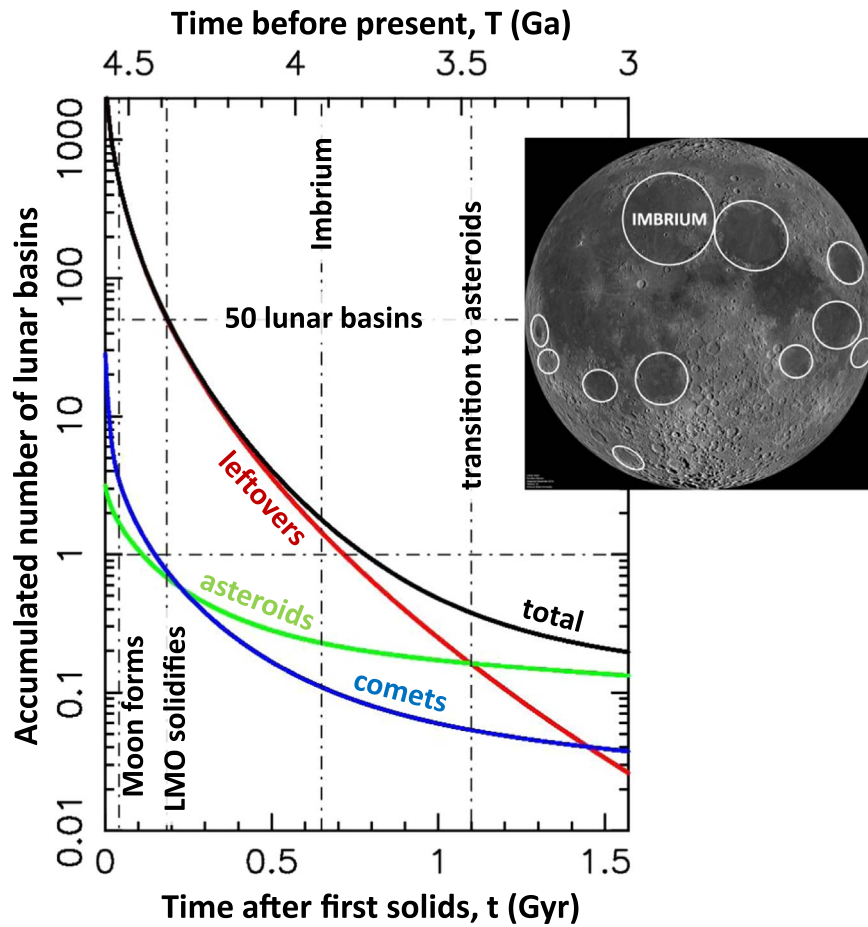
Figure 1. Early impacts of diameter $d > 20$ km planetesimals on the Moon match the number of known lunar basins—on the assumption that the basin record started at $t \simeq 190$ Myr. The plot shows the accumulated number of impacts after time t, where $t = 0$ is the birth of the solar system, and $t \simeq 4.57$ Gyr is the present time. The profiles have a declining trend as younger surfaces accumulate fewer impacts. The planetesimal, asteroid, and comet profiles are shown by red, green, and blue lines, respectively; the black line is the total impact flux. The vertical dashed–dotted lines show the lower bound on the Moon-forming impact ($t \sim 30$ Myr), estimated start of the lunar basin record ($t \simeq 190$ Myr or $T \simeq 4.38$ Ga), Imbrium formation ($t \simeq 650$ Myr or $T \simeq 3.92$ Ga), and transition from the planetesimal-dominated to asteroid-dominated impact stages ($t \simeq 1.1$ Gyr or $T \simeq 3.5$ Ga). The inset shows some of the lunar near-side basins.

distributed in a disk beyond Neptune, with Neptune on an initial orbit at 23 au. The bodies were given low orbital eccentricities, low inclinations, and the surface density $\Sigma(r) \propto r^{-1}$. The disk was truncated at 30 au to assure that Neptune stopped migrating near its current orbital radius at $\simeq 30$ au. The simulations were run from the time of the gas disk dispersal to the present epoch. The effects of outer planet (early) migration/instability, galactic tides, and perturbations from passing stars were accounted for in the model. The results were shown to be consistent with the orbital distribution of modern comets, Centaurs, and the Kuiper Belt.

The size distribution of outer disk cometesimals is calibrated from the number of large comets and Centaurs observed today, the size distributions of Jupiter Trojans and Kuiper-belt objects, and from the general condition that the initial setup leads to plausible migration/instability histories of the outer planets. The calibration gives $\sim 6 \times 10^9$ $d > 10$ km and $\sim 5 \times 10^7$ $d > 100$ km cometesimals in the original disk. The size distribution is expected to closely follow a power law with the cumulative index $\gamma \simeq -2.1$ for $10 < d < 100$ km, and have a transition to a much steeper slope for $d > 100$ km. The distribution is a product of the initial size distribution that was modified by collisional grinding. We account for the physical

lifetime of comets following the method described in Nesvorný et al. (2017b).

The impact flux of comets on the terrestrial worlds is computed with the Öpik algorithm (Bottke et al. 1994). The results of the Öpik code are normalized to the initial number of comets in the original disk (see above). The calibrated model gives us the flux of cometary impactors over the whole history of the Solar System. An excellent approximation of the cumulative impact flux of comets on the Earth is

$$F(d, t) = C_s(d)\{F_1 \exp[-(t/\tau_1)^{\alpha_1}]$$
$$+ F_2 \exp[-(t/\tau_2)^{\alpha_2}] + F_3(4570 - t)\}, \qquad (2)$$

with $F_1 = F_2 = 6.5 \times 10^3$, $\tau_1 = 7$ Myr, $\alpha_1 = 1$, $\tau_2 = 13$ Myr, $\alpha_2 = 0.44$, $F_3 = 4 \times 10^{-3}$ Myr^{-1}, $C_s(d) = 1$ for $d = 10$ km, and t in Myr.

3. Results

The integrated history of lunar impacts (Figure 1) shows that leftover planetesimals dominated the early impact flux ($t < 1.1$ Gyr or $T > 3.5$ Ga; T is measured looking backward from today). Asteroids took over and produced the most impacts in the last $\simeq 3.5$ Gyr. This may explain why the size distribution of modern lunar impactors is similar to NEAs, but

that of early impactors was not (Strom et al. 2005; Minton et al. 2015). The cometary flux was never large enough, in the whole history of the inner solar system, to be competitive. Indeed, the isotopic signatures of comets are difficult to find in lunar samples (Joy et al. 2012). The overwhelming majority of craters observed on the lunar surface must date back to $T > 3.5$ Ga, when the impact flux was orders of magnitude higher than it is today. The model predicts $\simeq 100$–500 $d > 20$ km impacts for $t > 30$–150 Myr ($T < 4.42$–4.54 Ga), which can be compared to only $\simeq 50$ known basins (Neumann et al. 2015). We therefore see that the number of impacts suggested by the model would be excessive if the Moon formed at $t = 30$–150 Myr (Kleine & Walker 2017) and recorded all large impacts since its formation.

This suggests that the lunar record is incomplete. The Moon was fully molten when it accreted from the debris disk created by the giant impact on proto-Earth (Canup et al. 2022). The subsequent evolution and solidification of the lunar magma ocean (LMO) was controlled by a number of geophysical processes, including tidal heating, formation of an insulating flotation crust and crust overturn (Meyer et al. 2010; Elkins-Tanton et al. 2011). The basins that formed when the LMO was still present would have extremely reduced topographic and crustal thickness signatures (Miljković et al. 2021); they may be unidentifiable today. Suppose, for example, that the lunar surface started recording basin-scale impacts at $t \simeq 190$ Myr ($T \simeq 4.38$ Ga)—the oldest known basins (e.g., South Pole–Aitken) would date back to this time. If so, the model implies that $\simeq 50$ $d > 20$ km impacts should be recorded (Figure 1), in close agreement with the number of known lunar basins. The estimated time of LMO solidification, $t = 160$–220 Myr or $T = 4.35$–4.41 Ga, is consistent with constraints from the radiogenic crustal ages and highly siderophile elements (HSEs) in the lunar mantle (Elkins-Tanton et al. 2011; Borg et al. 2015; Morbidelli et al. 2018; Zhu et al. 2019). A detailed analysis of HSEs will be published elsewhere (Nesvorný et al. 2022, in preparation).

Our impact model gives general support to empirically derived lunar chronologies (Neukum et al. 2001; Marchi et al. 2009; Robbins 2014), but differs in specifics (Figure 2). Classically, the lunar $N_1(T)$ chronology function—the number of accumulated $D > 1$ km craters in km^2 of the lunar surface since T—was obtained by fitting the measured crater densities on terrains with known radiometric ages. Neukum et al. (2001), for example, suggested $N_1(T) = a[\exp(bT) - 1] + cT$ with $a = 5.44 \times 10^{-14}$ km^{-2}, $b = 6.93$ Gyr^{-1}, and $c = 8.38 \times 10^{-4}$ Gyr^{-1} km^{-2}. The exponential term is identified here with the declining impact flux of leftover planetesimals (Figure 1). A *stretched* exponential function $\exp[-(t/\tau)^\alpha]$, however, more accurately approximates the declining flux in our simulations. The half-life of impact decline is $\delta t_{\text{half}} = \tau (t/\tau)^{1-\alpha}/(2\alpha)$, where $\tau = 1/b \simeq 144$ Myr and $\alpha = 1$ in Neukum et al. (2001), and $\tau = 6$ Myr and $\alpha = 0.45$ in this work. This gives fixed $\delta t_{\text{half}} \simeq 72$ Myr in the classical chronology, but changing half-life in our model (e.g., $t_{\text{half}} = 46$ Myr for $t = 200$ Myr and $t_{\text{half}} = 88$ Myr for $t = 650$ Myr).[5]

The Imbrium-era basins represent a crucial constraint on any impact chronology. In the model, $\simeq 0.31$ Imbrium-scale lunar impacts ($d \geqslant 100$ km; Miljković et al. 2013; Schultz &
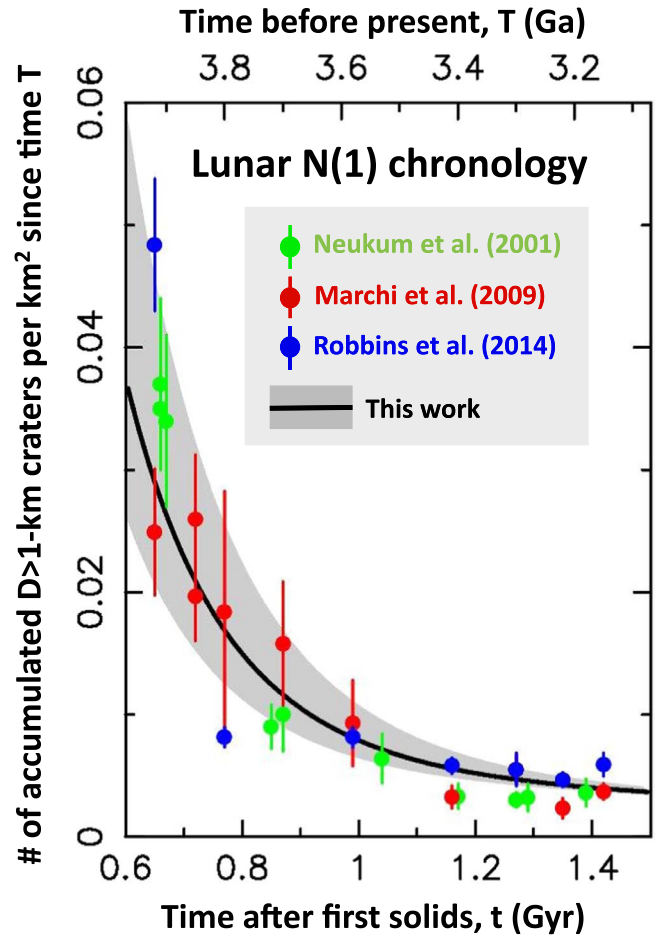

Figure 2. Our model N_1 chronology matches crater counts on lunar terrains with known radiometric ages. The bold solid line is $N_1(T) = a \exp[-(t/\tau)^\alpha] + cT$ with $t = 4570 - T$ (t and T in Myr), $a = 94$ km^{-2}, $\tau = 6$ Myr, $\alpha = 0.45$, and $c = 10^{-6}$ km^{-2} Myr^{-1}; the shaded area indicates the model uncertainty. The green (Neukum et al. 2001), red (Marchi et al. 2009), and blue dots (Robbins 2014) with associated error bars show different $D > 1$ km crater counts. The impact model also implies $\simeq 25$ $D > 20$ km craters per 10^6 km^2 for $T = 3.92$ Ga, in a close match to $N_{20} = 26 \pm 5$ reported for the Fra Mauro/Imbrium highlands (Orgel et al. 2018). The Nectaris basin with $N_{20} \simeq 170$ is estimated here to be $T = 4.21$–4.29 Gyr old.

Crawford 2016; Miljković et al. 2021) happen for $t > 600$ Myr. From the standard Poisson statistics, and folding in a generous ~50% uncertainty in the model flux calibration (Section 2), we estimate that the Imbrium formation was a 15%–35% probability event. This is low, but not an alarmingly low probability, especially because there is a very good reason for that. There are only two basins, Orientale and Schrödinger that formed after Imbrium. They were produced by $d \simeq 50$–64 km and $d \simeq 20$ km impactors, respectively (Johnson et al. 2016a; Miljković et al. 2016), which is consistent with the model expectation of ~2 basin-scale lunar impacts for $t > 600$ Myr (Figure 1). Having only two smaller basins with post-Imbrium formation ages, however, is surprising. For example, if the current asteroid-belt size distribution is adopted for reference, there should (on average) be ~7.4 $d > 20$ km impacts for every $d > 100$ km impact. This suggests that the Imbrium basin formed unusually late, by chance, to have only two smaller and younger basins than Imbrium (there would be many more younger/smaller basins otherwise), and justifies the 15%–35% probability of Imbrium formation quoted above. In

---

[5] There remain significant uncertainties about the character of the early chronology function. For example, Robbins (2014) found a very steep decay with $t_{\text{half}} = 22$–30 Myr for $t = 650$ Myr.
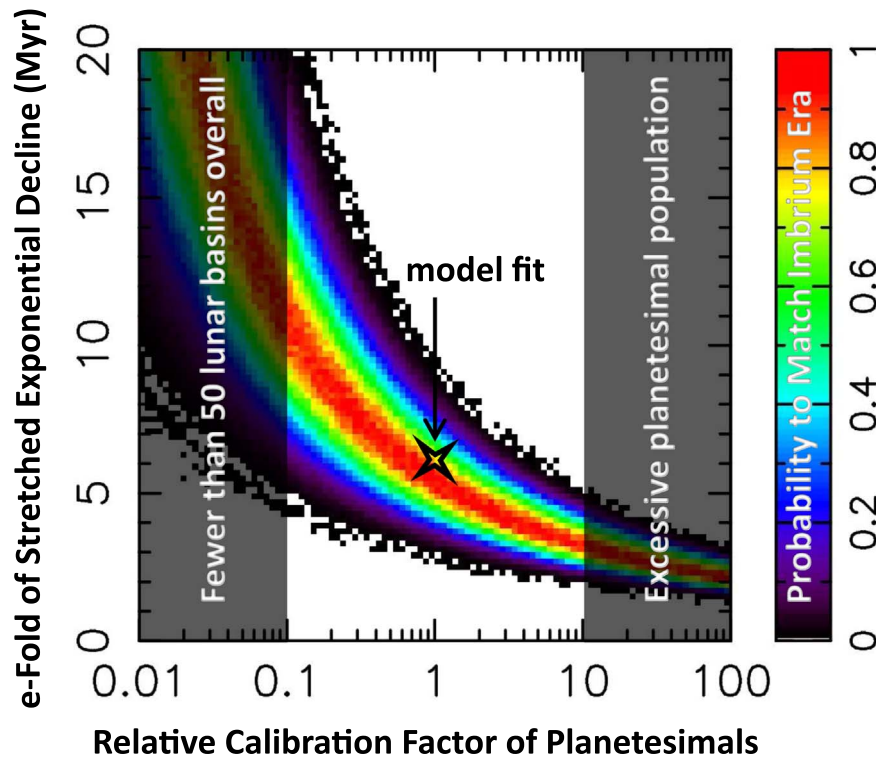
Figure 3. The model impact chronology satisfies Imbrium-era constraints. The rainbow plot shows the normalized probability for Imbrium to form late ($600 < t < 900$ Myr, $d > 100$ km) and have exactly two basins (Orientale and Schrödinger, $d > 20$ km impactors) younger than Imbrium. We fix $\alpha = 0.45$, and test different chronologies by varying the e-fold τ and relative calibration factor C_r, where $C_r = 1$ corresponds to the standard calibration of leftover planetesimals (Section 2.1). We generate a statistically large number of random impact sequences ($\sim 10^5$) for each pair (C_r, τ) and evaluate the likelihood of satisfying the condition described above. The likelihood is low if C_r and/or τ are small, because it is difficult to form Imbrium. It is low if C_r and/or τ are large, because more than one Imbrium forms and/or many smaller basins form after Imbrium. The star symbol denotes $C_r = 1$ and $\tau = 6$ Myr obtained from a fit to our simulation of leftover planetesimals.

fact, our impact chronology is (nearly) optimal to satisfy the Imbrium-era constraints (Figure 3).

The Earth receives $\simeq 20$ times more impacts than the Moon. When a large impactor strikes the Earth, it produces a vapor-rich ejecta plume. As the plume cools down, glassy spherules form and fall back, producing a global layer that can be several millimeters to many centimeters thick. Some ~ 16 spherule beds have been found in the late Archean period ($T = 2.5$–3.5 Ga; Marchi et al. 2021), although preservation biases and incomplete sampling may be an issue. At least some of these layers may have been produced by very large, $d \sim 50$ km impactors, but most are thought to record $d > 10$ km impacts (Marchi et al. 2010, Johnson et al. 2016b). This can be compared with the model predictions. We estimate $\simeq 20$ $d > 10$ km impacts on the Earth for $T = 2.5$–3.5 Ga (Figure 4), of which ~ 2 should be $d > 50$ km. The leftover planetesimals and main-belt asteroids contribute equally to impacts in this time interval (~ 10 impacts each). Whereas the asteroid impacts should be more uniformly spread over the late Archean, nearly all planetesimal impacts happen before ~ 3 Ga. The model gives ~ 10 and ~ 2 $d > 10$ km asteroid impacts on the Earth in the past 2.5 and 0.6 Gyr, respectively, which is consistent with the current impact flux of large NEAs (Nesvorný et al. 2021a).

Even though comets were dwarfed by planetesimals and asteroids in terms of the overall bombardment, evidence for cometary impacts can be found in the composition of Earth's atmosphere (Marty et al. 2016). Comets start to be released from the trans-Neptunian region near the onset of the outer planet instability. The cometary impact profile is found here to

be more extended in time than previously thought (Morbidelli et al. 2018), with 10% of cometary impacts happening at >55 Myr and 1% at >370 Myr after the instability. Adopting a case with the outer planet instability at $t < 10$ Myr and Moon formation at $t \sim 50$ Myr, we estimate that the Earth would have accreted $\sim 2 \times 10^{22}$ g of cometary material after the Moon-forming impact. This is consistent with comets being the main source of noble gases in the Earth's atmosphere (Marty et al. 2016; but a negligible source of Earth's water— the mass of Earth's oceans is 1.4×10^{24} g). In fact, the atmospheric abundance of noble gases can be used to constrain the delay between the outer planet instability and Moon formation, Δt. We estimate $20 < \Delta t < 60$ Myr, with the exact value depending on the physical lifetime of comets (Section 2). This suggests, if the instability happened very early ($t < 10$ Myr; Clement et al. 2018; Liu et al. 2022), that the Moon must have formed early as well ($t < 70$ Myr or $T > 4.5$ Gyr; Thiemens et al. 2019).

In a broader context, our work highlights the importance of impacts for the early Earth. The bulk of accreted mass was brought by 80–400 $d > 100$ km (Imbrium-scale) impacts and the stochastic accretion of very large planetesimals ($d \gtrsim 1{,}000$ km), as needed to explain Earth's HSEs (Bottke et al. 2010). If the surface of Earth's Hadean crust was widely reprocessed by these impacts, this could explain the age distribution of Hadean zircons and absence of terrestrial rocks older than 4.3 Gyr (Marchi et al. 2014). There is roughly a 50% chance that the last $d > 100$ km impact on the Earth happened as late as $T \lesssim 3.5$ Ga. In total, the early Earth received $\sim 2{,}000$–$10{,}000$
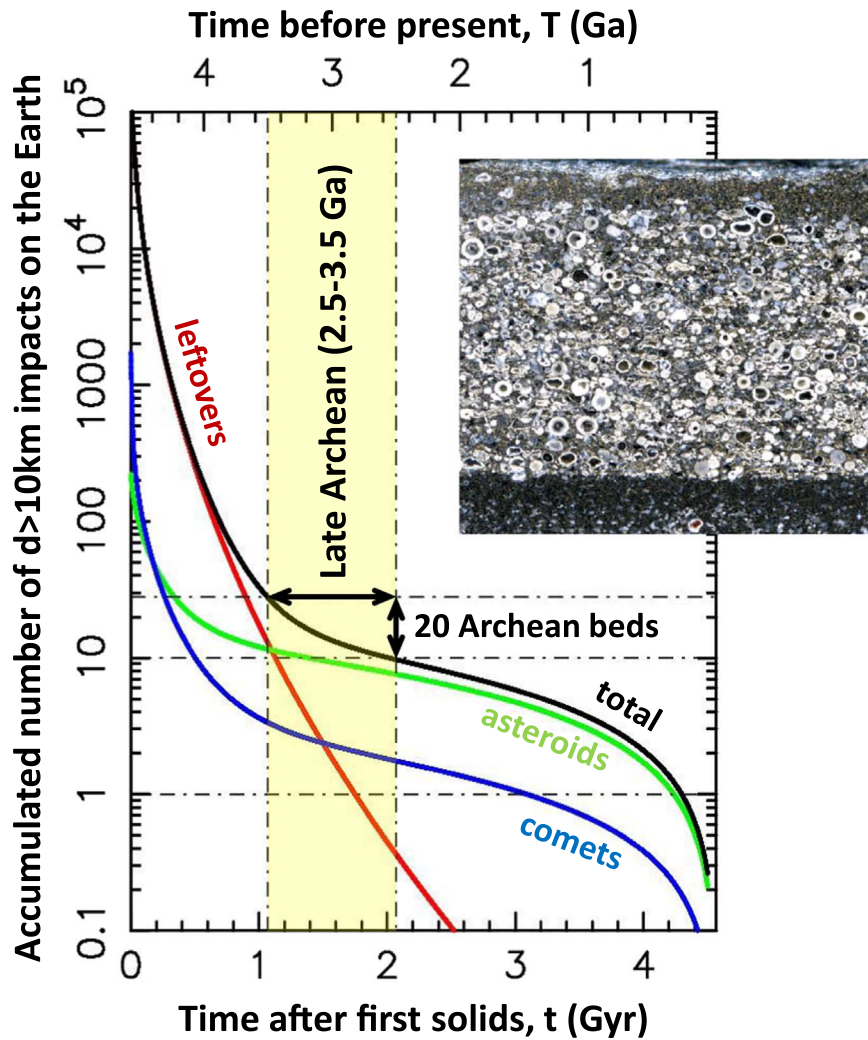
Figure 4. Model impacts of diameter $d > 10$ km bodies on the Earth match the number of Archean spherule beds. The vertical dashed–dotted lines outline the late Archean period, $T = 2.5$–3.5 Ga, where the model predicts $\simeq 20\ d > 10$ km impacts on the Earth. The sixteen known Archean spherule beds occur in two distinct time intervals, 2.4–2.7 Ga and 3.2–3.5 Ga (Marchi et al. 2021). If this is indicative of the average flux in the late Archean, there should be ~ 14 additional spherule beds at 2.7–3.2 Ga. If so, the number of $d > 10$ km impacts in the model would represent $\sim 60\%$ of the total number of spherule beds. For reference, some $\sim 43\ d > 7$ km impacts on the Earth are expected in the model at 2.5–3.5 Ga. The inset shows the Monteville spherule layer in South Africa (Reimold & Koeberl 2014).

$d > 10$ km impacts, each representing the magnitude of the Cretaceous–Paleogene (K/Pg) extinction-scale event (Alvarez et al. 1980). By $T \sim 3.7$ Ga, when we have the earliest firm evidence for biotic life (Nutman et al. 2016), the impact flux has already declined ~ 1000 times, and the mean interval between K/Pg-scale impacts stretched to > 1 Myr.

4. Conclusions

The main results of this work can be summarized as follows.

1. The leftover planetesimals produce most lunar impacts in the first 1.1 Gyr ($t < 1.1$ Gyr or $T > 3.5$ Ga). Asteroids produce most impacts in the last 3.5 Gyr. The transition from leftover planetesimals to asteroids has been imprinted in the crater size distributions (Strom et al. 2005, Head et al. 2010, Orgel et al. 2018). The comet contribution to the crater record is found to be insignificant (for the early instability case adopted here).

2. Some 500 $d > 20$ km planetesimals from the terrestrial planet zone (0.5–1.5 au) are expected to impact the Moon since its formation. The early crater record must have

been erased because the lunar surface was unable to support basin-scale impact structures. The ~ 50 known lunar basins formed after $t \simeq 160$–215 Myr ($T \lesssim 4.36$–4.41 Ga). This is consistent with the long-lived LMO (Morbidelli et al. 2018, Zhu et al. 2019). The South Pole–Aitken basin should date back to $T = 4.36$–4.41 Ga.

3. About two lunar basins are expected to form for $t \gtrsim 650$ Myr ($T \lesssim 3.92$ Ga). The Imbrium basin formation ($T \simeq 3.92$ Ga, $d \gtrsim 100$ km impactor) is estimated to happen with a 15%–35% probability in our model. Imbrium should have formed unusually late, relative to the expectations from the lunar impact chronology, to have only two smaller/younger basins than Imbrium (Orientale and Schrödinger); there would be many more younger/smaller basins otherwise.

4. The lunar chronology can be given as a sum of two terms: the stretched exponential function (the leftover planetesimal branch) and a constant (the asteroid or NEA branch). This is similar to the classical (empirical) crater chronologies (Neukum et al. 2001; Marchi et al. 2009;

Robbins [2014]), except that the cratering rate profile in the first $\sim$1 Gyr had a longer tail than the exact exponential. This can lead to modest, $\sim$50 Myr differences in the estimates of lunar basin ages.

5. Our model predicts $\simeq$20 $d > 10$ km impacts on the Earth for $T = 2.5$–3.5 Ga. This is similar to the number of known spherule beds in the late Archean (Bottke et al. [2012]; Johnson et al. [2016b]; Marchi et al. [2021]). Both the leftover planetesimals and main-belt asteroids contribute to impacts in this time interval. Whereas the asteroid impacts were more uniformly spread over the late Archean, nearly all planetesimal impacts should have happened before 3 Ga.
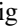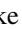
5. A Note on Previous Work

Bottke et al. ([2007]) studied lunar impacts of leftover planetesimals and concluded that the leftover planetesimals *cannot* produce basin-scale impacts on the Moon during the Imbrium era, because the collisional and dynamical decline of planetesimal impactors was presumably too quick. Comparing their impact profile with the ones obtained here, we identify the main reason behind this: the planetesimal population in Bottke et al. ([2007]) dynamically decayed by 2 orders of magnitude in the first 100 Myr. We do not find any such strong initial trend in our work. The problem in question is most likely related to the approximate nature of initial conditions in Bottke et al. ([2007]), where the present-day NEAs were used as a proxy for terrestrial planetesimals. We note that modern NEAs have relatively short dynamical lifetimes.

Brasser et al. ([2020]) developed a dynamical model for lunar impactors with four different components: E-belt, asteroid belt, comets, and leftover planetesimals. The main difference relative to our work is that their model was *not* absolutely calibrated from independent means. To match the lunar impact constraints in their model, Brasser et al. ([2020]) increased $\sim$10 times the population of the E-belt (see Bottke et al. [2012]), and suggested that the E-belt asteroids were the main source of basin-forming impacts. The best-fit contribution of planetesimals was found to be negligible; leftovers were therefore concluded to be only a minor source of lunar impacts. This can be compared to our work where we find the dominant role of leftover planetesimals.

ORCID iDs

David Nesvorný ⊙ https://orcid.org/0000-0002-4547-4301
Fernando V. Roig ⊙ https://orcid.org/0000-0001-7059-5116
David Vokrouhlický ⊙ https://orcid.org/0000-0002-6034-5452
William F. Bottke ⊙ https://orcid.org/0000-0002-1804-7814
Simone Marchi ⊙ https://orcid.org/0000-0003-2548-3291
Rogerio Deienno ⊙ https://orcid.org/0000-0001-6730-7857

References

Alvarez, L. W., Alvarez, W., Asaro, F., & Michel, H. V. 1980, Sci, 208, 1095
Benz, W., & Asphaug, E. 1999, Icar, 142, 5
Borg, L. E., Gaffney, A. M., & Shearer, C. K. 2015, M&PS, 50, 715
Bottke, W. F., Levison, H. F., Nesvorný, D., et al. 2007, Icar, 190, 203
Bottke, W. F., Nolan, M. C., Greenberg, R., & Kolvoord, R. A. 1994, Icar, 107, 255
Bottke, W. F., Vokrouhlický, D., Minton, D., et al. 2012, Natur, 485, 78
Bottke, W. F., Walker, R. J., Day, J. M. D., et al. 2010, Sci, 330, 1527
Brasser, R., Werner, S. C., & Mojzsis, S. J. 2020, Icar, 338, 113514
Canup, R. M., Righter, K., Dauphas, N., et al. 2022, arXiv:2103.02045
Chambers, J. E., & Wetherill, G. W. 1998, Icar, 136, 304
Clement, M. S., Kaib, N. A., Raymond, S. N., et al. 2018, Icar, 311, 340
Elkins-Tanton, L. T., Burgess, S., & Yin, Q.-Z. 2011, E&PSL, 304, 326
Fassett, C. I., Head, J. W., Kadish, S. J., et al. 2012, JGRE, 117, E00H06
Gomes, R., Levison, H. F., Tsiganis, K., & Morbidelli, A. 2005, Natur, 435, 466
Johnson, B. C., Blair, D. M., Collins, G. S., et al. 2016b, Sci, 354, 441
Johnson, B. C., Collins, G. S., Minton, D. A., et al. 2016a, Icar, 271, 350
Joy, K. H., Zolensky, M. E., Nagashima, K., et al. 2012, Sci, 336, 1426
Kaib, N. A., & Chambers, J. E. 2016, MNRAS, 455, 3561
Kleine, T., & Walker, R. J. 2017, AREPS, 45, 389
Levison, H. F., & Duncan, M. J. 1994, Icar, 108, 18
Liu, B., Raymond, S. N., & Jacobson, S. A. 2022, Natur, 604, 643
Mainzer, A. K., Bauer, J. M., Cutri, R. M., et al. 2019, PDSS
Marchi, S., Bottke, W. F., Elkins-Tanton, L. T., et al. 2014, Natur, 511, 578
Marchi, S., Drabon, N., Schulz, T., et al. 2021, NatGe, 14, 827
Marchi, S., Mottola, S., Cremonese, G., et al. 2009, AJ, 137, 4936
Marty, B., Avice, G., Sano, Y., et al. 2016, E&PSL, 441, 91
Meyer, J., Elkins-Tanton, L., & Wisdom, J. 2010, Icar, 208, 1
Miljković, K., Collins, G. S., Wieczorek, M. A., et al. 2016, JGRE, 121, 1695
Miljković, K., Wieczorek, M. A., Collins, G. S., et al. 2013, Sci, 342, 724
Miljković, K., Wieczorek, M. A., Laneuville, M., et al. 2021, NatCo, 12, 5433
Minton, D. A., Richardson, J. E., & Fassett, C. I. 2015, Icar, 247, 172
Morbidelli, A., Bottke, W. F., Nesvorný, D., et al. 2009, Icar, 204, 558
Morbidelli, A., Nesvorny, D., Laurenz, V., et al. 2018, Icar, 305, 262
Nesvorný, D., Bottke, W. F., & Marchi, S. 2021a, Icar, 368, 114621
Nesvorný, D., Roig, F., & Bottke, W. F. 2017a, AJ, 153, 103
Nesvorný, D., Roig, F. V., & Deienno, R. 2021b, AJ, 161, 50
Nesvorný, D., Vokrouhlický, D., Bottke, W. F., et al. 2018, NatAs, 2, 878
Nesvorný, D., Vokrouhlický, D., Dones, L., et al. 2017b, ApJ, 845, 27
Neukum, G., Ivanov, B. A., & Hartmann, W. K. 2001, SSRv, 96, 55
Neumann, G. A., Zuber, M. T., Wieczorek, M. A., et al. 2015, SciA, 1, e1500852
Nutman, A. P., Bennett, V. C., Friend, C. R. L., Van Kranendonk, M. J., & Chivas, A. R. 2016, Natur, 537, 535
Orgel, C., Michael, G., Fassett, C. I., et al. 2018, JGRE, 123, 748
Reimold, W. U., & Koeberl, C. 2014, JAfES, 93, 57
Robbins, S. J. 2014, E&PSL, 403, 188
Schultz, P. H., & Crawford, D. A. 2016, Natur, 535, 391
Strom, R. G., Malhotra, R., Ito, T., Yoshida, F., & Kring, D. A. 2005, Sci, 309, 1847
Tera, F., Papanastassiou, D. A., & Wasserburg, G. J. 1974, E&PSL, 22, 1
Thiemens, M. M., Sprung, P., Fonseca, R. O. C., et al. 2019, NatGe, 12, 696
Tsiganis, K., Gomes, R., Morbidelli, A., & Levison, H. F. 2005, Natur, 435, 459
Wetherill, G. W. 1990, AREPS, 18, 205
Youdin, A. N., & Goodman, J. 2005, ApJ, 620, 459
Zhang, B., Lin, Y., Moser, D. E., et al. 2019, JGRE, 124, 3205
Zhu, M.-H., Wünnemann, K., Potter, R. W. K., et al. 2019, JGRE, 124, 2117